PAPER

Check for updates

Two-stage metal ion sensing by through-space and through-bond charge transfer†

Guoxin Yin,‡[a] Yu Wang,‡[a] Yuping Yuan, ID ‡[ab] Ruxue Li,[c] Rui Chen ID [c] and Hsing-Lin Wang ID *[a]

A highly selective colorimetric and ratiometric "two-stage"/"off−on" type fluorescent probe with an ability to exclude other heavy and transition metal ions has been designed and synthesized. Low concentrations of Fe^{3+} cause through-space charge transfer which leads to fluorescence quenching exceeds 96%, and a further increase of Fe^{3+} concentration results in the formation of a complex with the maximum emission peak of 1,3-bis((E)-2-(pyridin-4-yl)vinyl)-2-methoxy benzene (BPVMB) being shifted largely by 100 nm (from 416 to 516 nm), which was examined by fluorescence, absorption detection and femtosecond transient absorption measurements on the basis of intramolecular charge transfer (ICT).

Introduction

In recent years, the synthesis and design of highly selective and sensitive sensors for heavy and transition metal ions have received wide attention because of their biological, environmental and industrial applications.[1–6] Among various metal ions, iron is the most abundant and crucial transition element in the human body and plays an important role in physiological processes such as electron transfer, oxygen uptake, gene expression and oxygen metabolism.[7] Overload or deficiency of iron can cause a series of human diseases.[8–13] The third most abundant metal copper in the human body is also an essential trace element. Excess copper can often be toxic to certain biological systems and is associated with various neurodegenerative disorders including Wilson's disease and Alzheimer's disease.[14,15] On the other hand, water and soil contamination by metal ions including iron, copper and other metals has attracted widespread interest as it has posed a threat to our daily life. Thus, it is important to detect and quantify those metal ions in both biological and environmental systems. Current detective determination methods for Fe^{3+} such as atomic absorption spectroscopy, mass spectrometry and electrochemical

spectroscopic analyses suffer either from their elaborate and sophisticated nature or from time consuming experiments.[16–19] In contrast, fluorescence methods are increasingly being called upon due to their conveniences and high sensitivity.[20]

To date, it is still difficult for most sensing platforms to distinguish Cu^{2+} and Fe^{3+}. For most of the reported fluorescent sensors of Cu^{2+} and Fe^{3+}, binding of the metal ion causes quenching of the fluorescence emission due to their paramagnetic nature.[20–24] Only a few sensors in which the binding of Fe^{3+} causes an increase in the fluorescence intensity or change in wavelength have been reported. Rhodamine-B based sensors have been reported as "turn-on" fluorescent and colorimetric sensors for Cu^{2+}, Al^{3+} and Fe^{3+}. However, the chemosensor cannot differentiate Cu^{2+}, Fe^{3+} and Al^{3+}.[25,26] In this regard, ratiometric and colorimetric measurements are more attractive to achieve higher selectivity and sensitivity upon binding of Fe^{3+} to the receptor. Ratiometric measurements have important features that measure the analyte concentration and minimize the measurement errors.[27,28] However, up to now, few colorimetric and ratiometric fluorescent chemosensors for Fe^{3+} have been found in the literature. To the best of our knowledge, most of the reported Fe^{3+} sensors are based on an assumption of the intramolecular charge transfer (ICT) mechanism which has not been proved yet.

In this manuscript, we present a novel sensing platform: a two-stage ratiometric and colorimetric fluorescent chemosensor with high Fe^{3+} selectivity. By varying the concentration of Fe^{3+}, it is possible to produce through-space charge transfer quenching followed by fluorescence turn-on with a large red shift of about 100 nm.[29–33] At first, the addition of Fe^{3+} induced fluorescence quenching due to the through space charge transfer. Then binding of Fe^{3+} to the pyridyl group of BPVMB induced a large red shift in fluorescence emission spectra due to

[a] *Department of Materials Science and Engineering, Southern University of Science and Technology, 1088 Xueyuan Avenue, Shenzhen, 518055, P. R. China. E-mail: wangxl3@sustech.edu.cn*
[b] *Academy for Advanced Interdisciplinary Studies, Southern University of Science and Technology, 1088 Xueyuan Avenue, Shenzhen, 518055, P. R. China*
[c] *Department of Electrical and Electronic Engineering, Southern University of Science and Technology, 1088 Xueyuan Avenue, Shenzhen, 518055, P. R. China*
† Electronic supplementary information (ESI) available: Synthesis and corresponding characterization data for BPVMB about absorption titration spectra, titration profile, fluorescence intensity, and ^{1}H and ^{13}C spectra. See DOI: 10.1039/d0tc01082k
‡ These authors contributed equally to this work.

intramolecular charge transfer (ICT). Such a turn off and then green emission will be useful in applications as it can detect the existence of different Fe^{3+} concentrations. An ICT mechanism for our system is further proved by femtosecond transient absorption measurements. Furthermore, high sensitivity for Fe^{3+} was achieved *via* the replacement method.

Experimental section

Materials

Acetonitrile, tetrahydrofuran and all the chloride salts of metal ions were obtained from Aldrich. All other reagents and solvents utilized in the experiments were of reagent and spectroscopic grades and used as received without further purification.

Measurements of UV and PL

UV absorption spectra were obtained on a Cary 5000 UV-vis-NIR spectrophotometer. Fluorescence emission spectra were obtained using a HORIBA PTI-QM-8075 luminescence spectrometer. A 1 cm width and 3.5 cm height quartz cuvette was used. The metal ion (Na^+, Mg^{2+}, Ca^{2+}, Pb^{2+}, Cd^{2+}, Mn^{2+}, Ni^{2+}, Cu^{2+}, Zn^{2+} and Fe^{3+}) stock solutions were prepared in acetonitrile in the order of 4 mM. Ligand BPVMB stock solutions were prepared (C = 1 mM) in acetonitrile. Working solutions of ligands and metal ions were freshly prepared from the stock solutions. The excitations were carried out at 320 nm for ligand BPVMB with 3 nm emission slit widths.

Measurements of femtosecond transient absorption (TA) spectra

The TA spectra and dynamics were recorded using a standard pump–probe configuration at 350 nm, ∼100 fs pump pulses at a 1 kHz repetition rate, and a broad-band white-light super-continuum probe (18SI80466 Rev.1, Newport). The excited power was 4 mW and the spot diameter was 300 μm.

Synthesis of BPVMB

1,3-Diiodo-2-methoxybenzene (500 mg, 1.39 mmol) and 4-vinylpyridine (0.3 mL, 2.78 mmol) were dissolved in 10 mL of *N*,*N*-dimethylformamide and 10 mL of diisopropylethyl-amine in a flask. The mixture was bubbled with N_2 for 20 min and palladium acetate (15.7 mg, 0.07 mmol) and tris(2-methyl-phenyl)phosphine (30.4 mg, 0.1 mmol) were added into the mixture under N_2 flow. The reaction was stirred at 100 °C under N_2 for 24 h. The reaction was cooled to room temperature and filtered through Celite. The filtrate was collected and evaporated in a vacuum. The crude product was purified by column chroma-tography with methanol/ethyl acetate (1:4 volume ratio) as the eluent. After removing the solvent, 340.5 mg of white crystal was collected with a yield of 78%. ^{1}H-NMR (400 MHz, $CDCl_3$), δ 8.59 (d, 4H, J = 8 Hz), 7.63 (d, 2H, J = 4 Hz), 7.61 (d, 2H, J = 4 Hz), 7.40 (d, 4H, J = 8 Hz), 7.20 (t, 1H, J = 8 Hz), 7.07 (d, 2H, J = 16 Hz), 3.81 (s, 3H); ^{13}C-NMR (100 MHz, $CDCl_3$), δ 156.65, 150.29, 144.71, 130.37, 123.73, 127.32, 127.11, 124.84, 120.98, 62.61. The synthesis route is shown as below (Scheme 1).
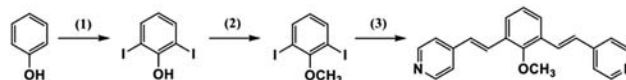
Scheme 1 Synthetic scheme of BPVMB. (1) Iodine, H_2O, r.t.; (2) iodo-methane, acetone, reflux; (3) palladium acetate, triphenyl-phosphine, 4-vinylpyridine, *N*,*N*′-dimethylformamide.

Determination of apparent dissociation constant

Fluorescence spectroscopy was used to determine the apparent dissociation constants (K_d) of BPVMB (50 μM) with Zn^{2+} and Cd^{2+}, using the reported method.[27] The fluorescence intensity data were fitted to eqn (1), and K_d was calculated:

$$F = F_0 + (F_{max} - F_0)\frac{[M^{3+}]_{free}}{K_d + [M^{3+}]_{free}} \quad (1)$$

where F is the fluorescence intensity, F_{max} is the maximum fluorescence intensity, F_0 is the fluorescence intensity with no addition of Fe^{3+} and Cu^{2+}, and $[M^{3+}]_{free}$ is the free Fe^{3+} and Cu^{2+} concentration.

Results and discussion

Effect of solvent on the fluorescence of BPVMB

The UV-absorption and fluorescence spectra of BPVMB in tetrahydrofuran, dimethyl sulfoxide, methanol, chloroform, ethanol, ethyl acetate, dimethylformamide and acetonitrile were measured and the results are shown in Fig. 1. All solutions exhibit blue emission without the addition of metal ions (Fig. 1b). The absorption spectra of all solutions exhibit a peak value at around 305 nm (Fig. 1c) and in detail the absorbance peaks of BPVMB in tetrahydrofuran, dimethyl sulfoxide, methanol, chloroform, ethanol, ethyl acetate, dimethylformamide and aceto-nitrile are at 305, 312, 306, 306, 307, 302, 307 and 304 nm, respectively. The emission spectra of BPVMB in these solvents show the peak value at the wavelength range from 420 to 428 nm.
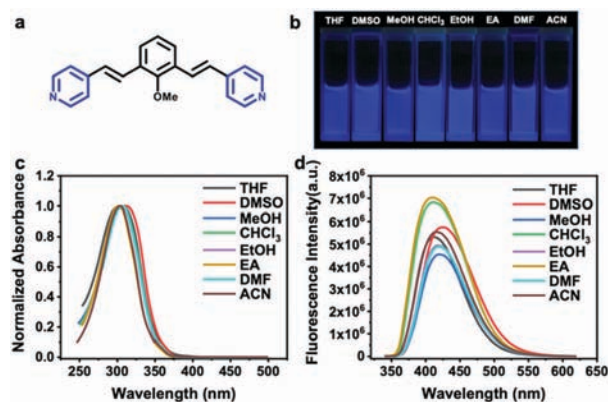

Fig. 1 (a) Molecular structure of BPVMB. (b) Fluorescence emission of BPVMB in different solvents (tetrahydrofuran, dimethyl sulfoxide, methanol, chloroform, ethanol, ethyl acetate, dimethylformamide and acetonitrile). (c) Plot of normalized absorbance of BPVMB in different solvents. (d) Fluorescence emission spectra of BPVMB (0.1 mM) ($\lambda_{ex.}$ = 320 nm) in different solvents.

The small changes in both UV absorption and fluorescence spectra indicate the negligible solvatochromatism property of BPV MB (Fig. 1d).

Fe^{3+} selectivity

In order to evaluate the metal ion sensing properties of BPVMB, we first examined the optical property of BPVMB solutions with various metal ions (including Na$^+$, Mg^{2+}, Ca^{2+}, Pb^{2+}, Cd^{2+}, Mn^{2+}, Ni^{2+}, Cu^{2+}, Zn^{2+} and Fe^{3+}) in acetonitrile. Fluorescence emission of BPVMB upon addition of metal ions is shown in Fig. 2a. The Cu^{2+} and Ni^{2+} could cause fluorescence quenching,

while Zn^{2+} and Cd^{2+} induce a slight red shift in fluorescence from 400 nm to $\sim$460 nm (blue fluorescence), while Fe^{3+} causes a red-shift to 530 nm (green fluorescent); such a red shift enables BPVMB to easily distinguish Fe^{3+} among other metal ions, even through the naked eye.

In contrast, BPVMB responds differently with respect to various metal ions in tetrahydrofuran solutions, see Fig. 2d. Quenching of fluorescence was observed after addition of Ni^{2+} and Fe^{3+}, while there is no change in emission color upon addition of various metal ions. Of particular interest is Cu^{2+} which leads to fluorescence quenching in acetonitrile, yet in
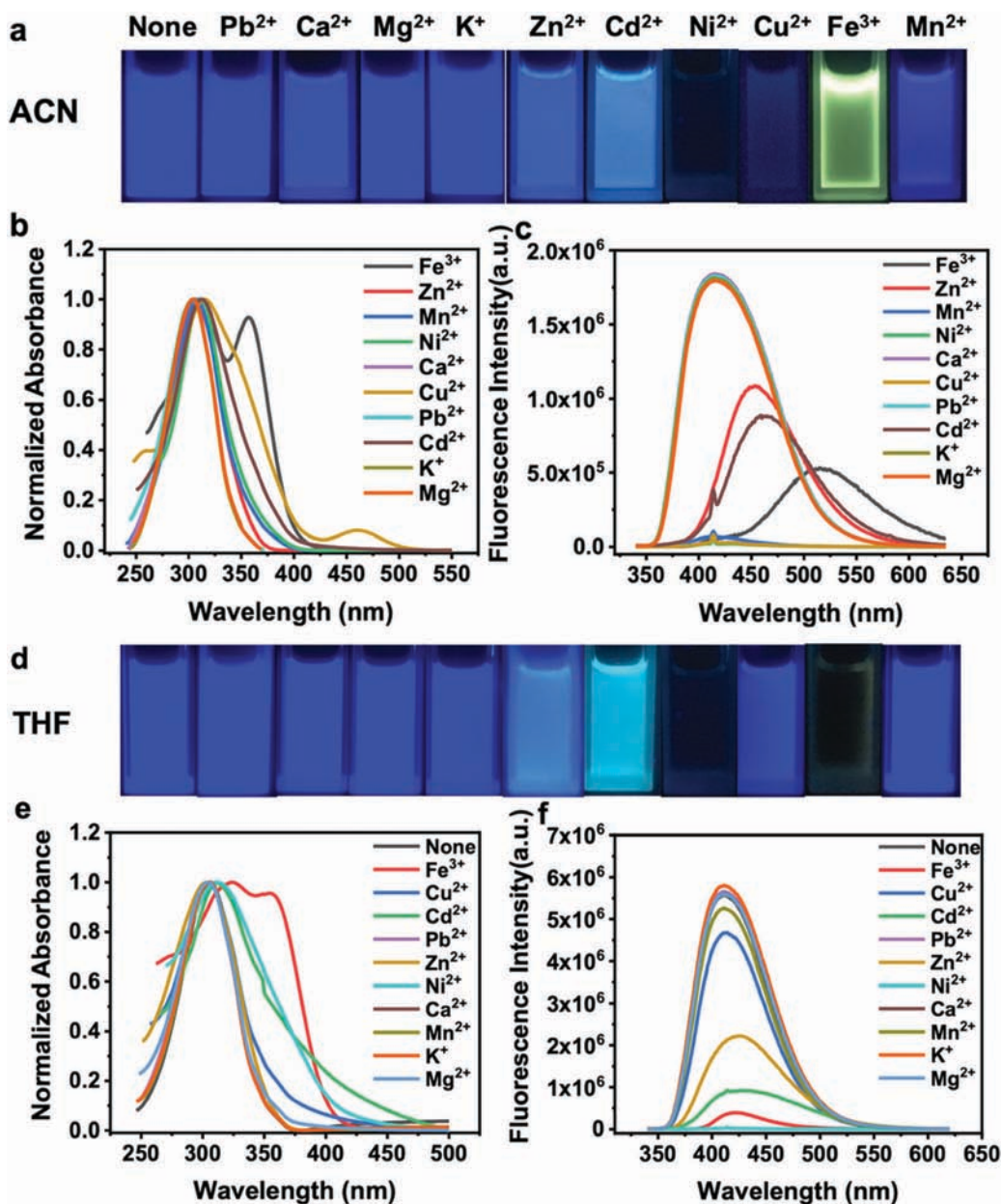

Fig. 2 (a) Changes in the fluorescence emission due to BPVMB (50 μM) in the presence of 4 mM of various added cations under a UV lamp (365 nm) in acetonitrile. (b) UV-vis spectra and (c) fluorescence spectra of BPVMB (50 μM) in acetonitrile and in the presence of various added cations (4 mM). (d) Changes in the fluorescence emission due to BPVMB (50 μM) in the presence of 4 mM of various added cations under a UV lamp (365 nm) in tetrahydrofuran. (e) UV-vis spectra and (f) fluorescence spectra of BPVMB (50 μM) in tetrahydrofuran and in the presence of various added cations (4 mM).

14030 | J. Mater. Chem. C, 2020, 8, 14028–14036

This journal is © The Royal Society of Chemistry 2020

tetrahydrofuran, it has almost no effect on the fluorescence of BPVMB. Such a phenomenon suggests that electronic coupling between BPVMB and Cu^{2+} and Fe^{3+} to certain extent is solvent-dependent.

To validate the feasibility of using BPVMB as an Fe^{3+} selective fluorescent sensor, we have carried out anti-interference experiments in the presence of various metal ions (Fig. 3). When BPVMB was treated with 5 equiv. of Fe^{3+} in the presence of other metal ions (Mg^{2+}, K^+, Cd^{2+}, Ca^{2+}, Zn^{2+}, Cu^{2+}, Ni^{2+}, Pb^{2+}, Mn^{2+}, Cr^{3+} and Al^{3+}) with the same concentration, Cd^{2+} and Mn^{2+} inhibited about 60% of the interaction between BPVMB and Fe^{3+} ions judging from the change of F_{516}/F_{416}. Therefore, BPVMB can be used as a selective fluorescent sensor for Fe^{3+} in the presence of these competing metal ions tested in this work.

In order to understand the fluorescence response of BPVMB to Fe^{3+}, the absorption and fluorescence emission spectra with different Fe^{3+} concentrations were recorded. The absorption spectrum exhibits a peak value at 300 nm for BPVMB in acetonitrile and peak values at 240 nm, 320 nm, and 360 nm for Fe^{3+} in acetonitrile (Fig. S1, ESI†). Upon addition of 10 μM Fe^{3+} to the BPVMB solution, the absorbance at ~300 nm gradually red-shifts and eventually disappears with a concomitant increase of two new peaks at 240 nm and 360 nm. These two peaks are due to the increasing concentration of Fe^{3+} (Fig. S2, ESI†). The isosbestic points at 275 nm and 325 nm indicate that the spectral change is due to relative compositional changes between BPVMB and Fe^{3+}. Fluorescence emission spectra of BPVMB is shown in Fig. S3 (ESI†) upon excitation at 350 nm. Upon addition of Fe^{3+}, the fluorescence intensity at 416 nm decreases until the concentration ratio of BPVMB and Fe^{3+} reaches 1:2. With continuous addition of aliquots of Fe^{3+} based on the concentration ratio of BPVMB and

Fig. 3 Competitive selectivity of BPVMB toward Fe^{3+} in the presence of other metal ions. The emission ratio at 516 and 416 nm (F_{516}/F_{416}) of PBVMB (S.) (50 μM) in acetonitrile induced by indicated metal ions. The final concentration of Fe^{3+}, Mg^{2+}, K^+, Cd^{2+}, Ca^{2+}, Zn^{2+}, Cu^{2+}, Ni^{2+}, Pb^{2+}, Mn^{2+}, Cr^{3+} and Al^{3+} is 250 μM. Excitation was at 350 nm. S. = free sensor (PBVMB).

Fe^{3+} from 1:2 to 1:4, a red-shifted broad emission band centered at 516 nm increases gradually. Fluorescence detection limits of BPVMB for Fe^{3+} were determined from the linear plot of F_{516}/F_{416} versus $[Fe^{3+}]$ in acetonitrile solution (Fig. S11, ESI†). The detection limit is 13.109 μM calculated on the basis of $3\sigma/K$.[34]

The above results suggest charge transfer between Fe^{3+} and BPVMB where BPVMB acts as an electron donor and Fe^{3+} serves as an electron acceptor. We hypothesize this to be a two stage process. At this first stage, which occurs at a low Fe^{3+} concentration, charge transfer through space between Fe^{3+} and BPVMB causes quenching of the fluorescence (Fig. 4a). Upon increasing the concentration of Fe^{3+} from 0 to 0.6 μM, a significant decrease in 416 nm emission was observed (Fig. 4c). The upward curvature of the Stern–volmer plot (Fig. S4, ESI†) is typical for situations in which both dynamic quenching and static quenching occur.[35] Such a type of plot indicates a complex interaction mechanism, which indicates the presence of specific binding interactions and more than one quenching processes: concomitant through space charge transfer and intramolecular charge transfer in this situation.[36] This is consistent with our hypothesis that both the complex between the BPVMB and the Fe^{3+} ions and the non-complexed Fe^{3+} formed during static and dynamic quenching.

Upon addition of Fe^{3+} to a BPVMB solution of 0.6 μM, a red-shifted broad emission band centered at 530 nm increases gradually (Fig. 4d), which is highly likely due to the BPVMB–Fe^{3+} complex formation through bonding of the pyridine moiety with Fe^{3+}. Therefore, we propose that the large red shift in the second stage is dominated by intramolecular charge transfer among BPVMB and Fe^{3+} (Fig. 4b). The disassociation constants (K_d) of BPVMB with Fe^{3+} in these two stages at 416 nm and 516 nm were determined by emission spectroscopy (Fig. S5, ESI†) to be 9.5×10^{-4} and 1.07×10^{-4}, respectively.[27] The smaller dissociation constant for the second stage might indicate the BPVMB–Fe^{3+} complex formation at a higher Fe^{3+} concentration.

In order to analyse the carrier kinetics between iron ions and BPVMB, the details of pump–probe TA spectra are described in Fig. 5. A pump pulse at 350 nm (~100 fs and 1 kHz) was used to excite the BPVMB and different proportions of BPVMB:Fe^{3+} solution. The induced absorption changes (ΔOD) as a function of both wavelength and time were monitored by a white light continuum probe pulse, providing a complete record of charge transfer and recombination processes. In Fig. 5a, the TA spectra of the different proportions of BPVMB:Fe^{3+} solution at 2 ps are shown. In the picture, it can be seen that there are four obvious ultrafast signals, namely two negative signals at about 360 and 550 nm, and two positive signals at about 420 and 650 nm, respectively. The peak of 360 nm consists of a major band of ground-state bleaching (GSB) from the absorption of Fe^{3+} that is not present in the signal of the BPVMB sample, while for the peak of 550 nm, it close to the PL peak position of green light emission of the BPVMB:Fe samples with a ratio of more than 1:2 according to Fig. S3 (ESI†) (a little red shift may come from the thermal effect), indicating that this peak is derived from the stimulated emission (SE) of a new combining state between
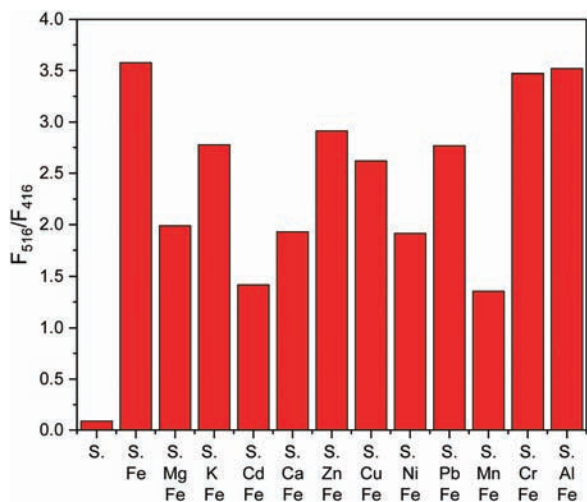
This journal is © The Royal Society of Chemistry 2020

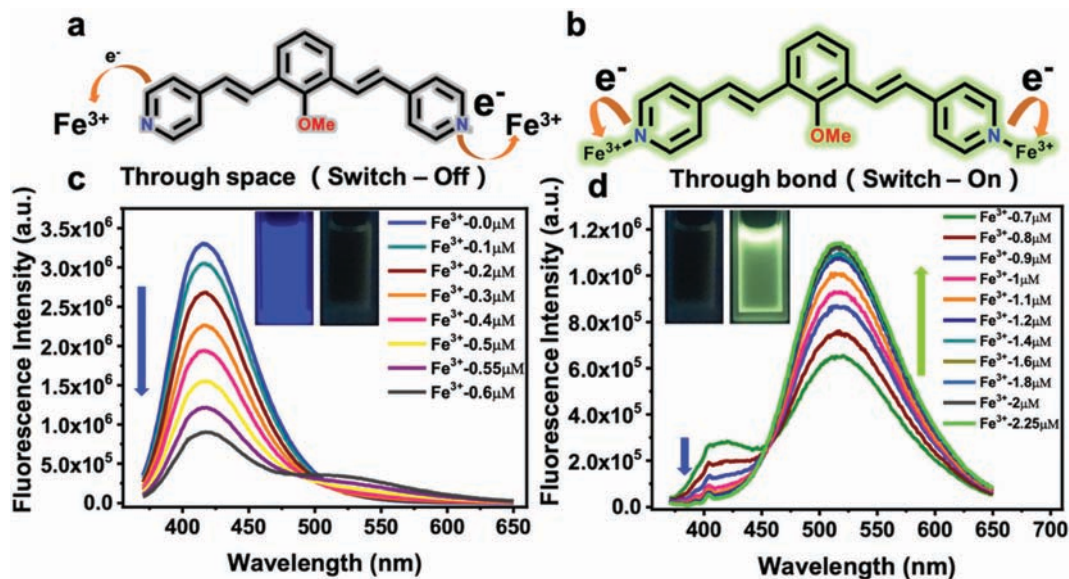*J. Mater. Chem. C*, 2020, **8**, 14028–14036 | **14031**

Fig. 4 (a) Schematic representation of the through-space charge transfer leading to fluorescence quenching at lower Fe^{3+} concentrations (the first stage); (b) formation of an intramolecular charge transfer complex at higher concentrations (the second stage); (c) fluorescence quenching of BPVMB in the presence of low Fe^{3+} concentrations, from 0 to 6 μM Fe^{3+}; "turn off" and (d) "turn-on" states with a large red shift from 415 nm to 520 nm at higher Fe^{3+} concentrations.

BPVMB and Fe (the PL emission peak of the pure Fe^{3+} solution is at 415 nm and is very weak). The peak at about 650 nm is derived from excited state absorption (ESA) of Fe^{3+}, while the peak at about 420 nm is a more important signal in the BPVMB:Fe^{3+} samples, which is derived from ESA of BPVMB and charge transfer (CT) from BPVMB to Fe^{3+} (this CT process will be described in detail below). In addition, it is worth noting that with an increase in the concentration of Fe ions in the BPVMB:Fe^{3+} samples, the peak position of about 420 nm gradually blue-shifts as shown in Fig. 5b. This implies that the CT from BPVMB to Fe^{3+} gradually increases with the increase of Fe^{3+} concentration, and finally reaches a saturation value. It is well known that the CT often occurs within 20 ps. In order to focus on this process, the BPVMB:Fe^{3+} = 1:3 sample with a more obvious transfer signal is selected for detailed analysis, which is shown in Fig. 5c. Obviously, the GSB signal shows a little change within 20 ps implying that the electrons from excited states have not yet returned to the ground states. However, the positive signal at 418 nm is significantly reduced while the signal at 460 nm is significantly increased. In addition, the positive signal at about 418 nm is gradually blue shifted. In Fig. 5d, all of the signals gradually return to the ground state after 20 ps. This phenomenon verifies that there is CT between BPVMB and Fe^{3+}, and the charge carrier dynamics in the BPVMB:Fe^{3+} samples are shown in Fig. 5.

Fig. 6a shows the ground states and excited states of BPVMB and Fe^{3+} and the new combining state between BPVMB and Fe^{3+}. After being excited by 350 nm, GSB, ESA, CT and SE processes occur in the sample, which have been mentioned above. Among them, the process of CT from BPVMB to Fe^{3+} will occur after Fe^{3+} was added, but it may have two cases that at low

and high concentrations, respectively. At a low concentration of Fe^{3+} (BPVMB:Fe^{3+} < 1:2), BPVMB and Fe^{3+} are not combined due to the relatively low binding constant, and the CT from BPVMB to Fe^{3+} is only through space (space charge transfer: SCT, and the positions of BPVMB and Fe^{3+} gradually approach with an increase in the concentration of Fe^{3+}). However, most of those carriers will undergo non-radiative recombination in Fe^{3+}, resulting in quenching of the PL. While at a high concentration of Fe^{3+} (BPVMB:Fe^{3+} > 1:2), the CT from BPVMB to Fe^{3+} will be transferred through the new combined state (binding charge transfer: BCT), as shown in Fig. 6a. When the charges transferred from BPVMB to Fe^{3+}, a positive signal at about 418 nm will appear, and then the carrier transfer to about 460 nm through intraband relaxation, thereby participating in the radiation recombination of Fe^{3+} that produces 550 nm green light emission. It can be noted that with the increase of Fe^{3+} concentration and time (within 20 ps), the peak position near 420 nm gradually blue shifts. This is due to the charge accumulation before they transferred to the state of 460 nm. Thus, the intensity of ∼418 nm will decrease and that of ∼460 nm will increase. The transient signal of the BPVMB and the ground state after 20 ps. This phenomenon verifies that there is CT between BPVMB and Fe^{3+}, and the charge carrier dynamics BPVMB:Fe^{3+} = 1:3 solution at 418 nm and 460 nm represent the kinetics of this process. The solid lines are multiexponential fits to these kinetics, are shown in Fig. 6b and Table 1.

It can be seen that the BPVMB sample has two lifetime components that may come from the ESA and SE (0.36 and 2480 ps, respectively). Note that those two lifetime components, each occupy ∼50% that gives rise to a very weak TA signal of BPVMB. After the Fe^{3+} was added, the system has one more
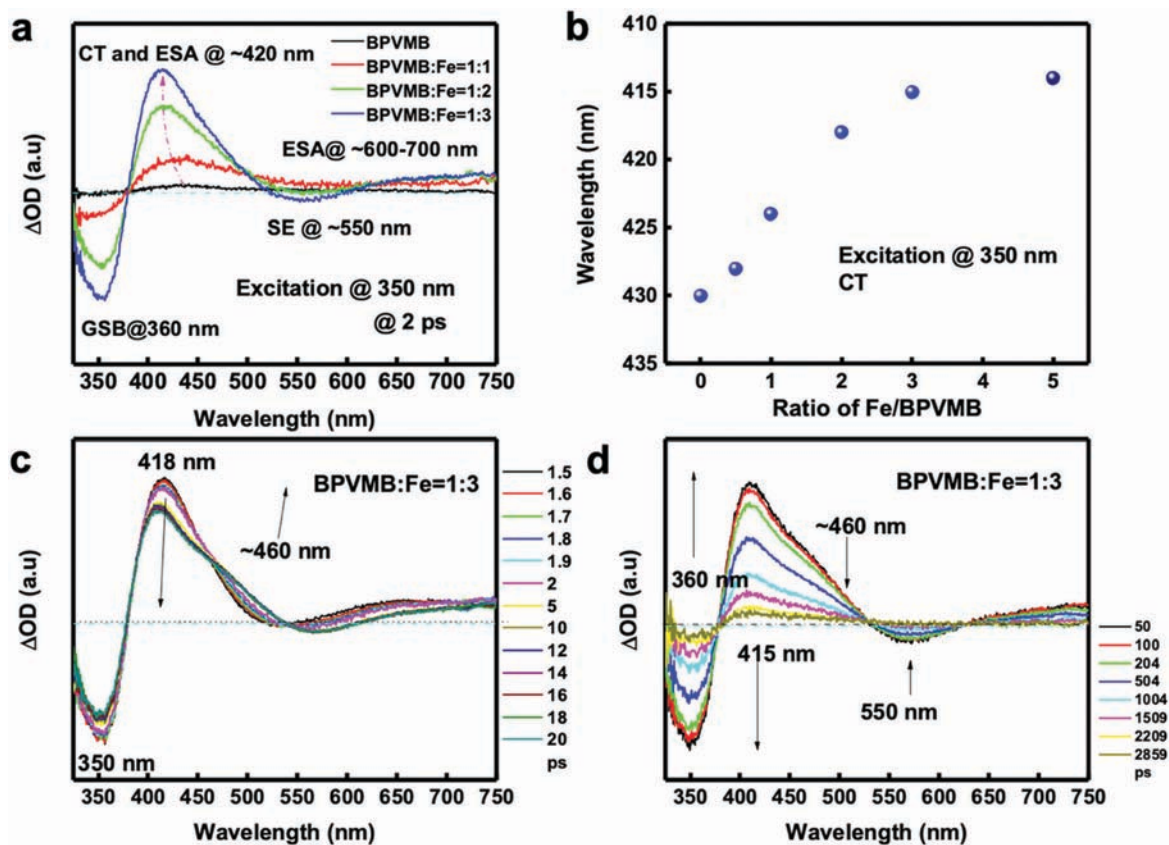
Fig. 5 TA spectra and kinetics of BPVMB and BPVMB : Fe^{3+} solution measured with 350 nm excitation. (a) TA spectra of BPVMB and different proportions of BPVMB : Fe^{3+} solution at 2 ps. (b) Peak positions of different proportions of BPVMB:Fe^{3+} solution at about 418 nm. (c) and (d) TA spectra of BPVMB : Fe^{3+} = 1 : 3 solution within and after 20 ps.
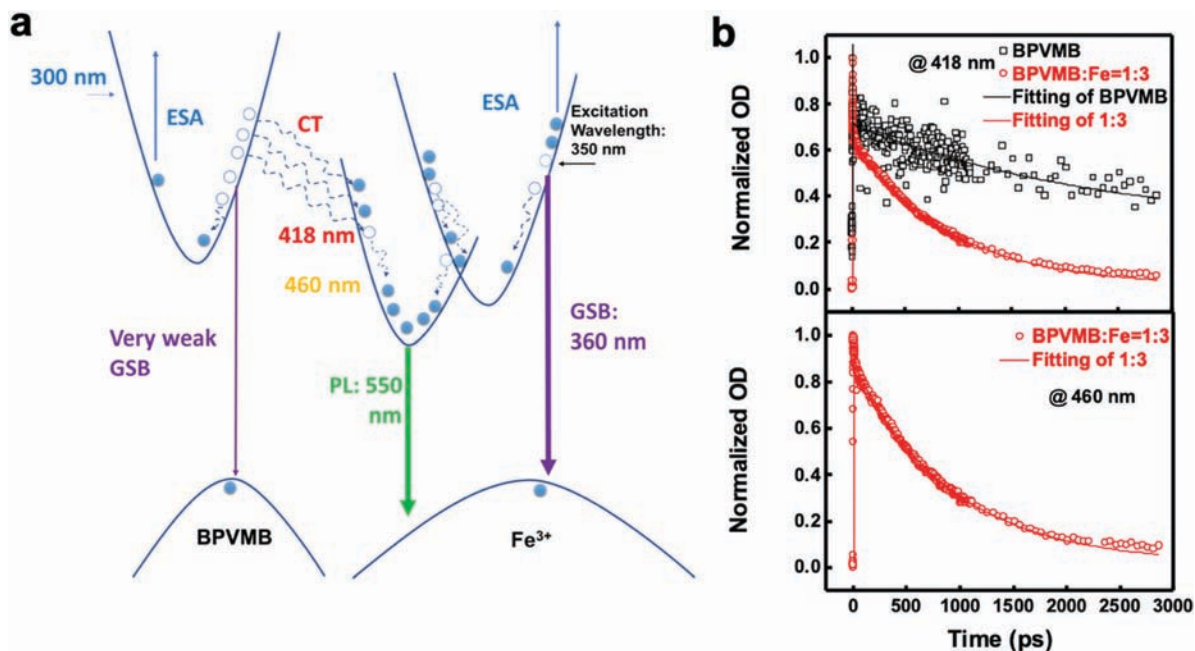

Fig. 6 (a) Schematic illustration of charge carrier dynamics in the BPVMB:Fe^{3+} samples. (b) Kinetics of transient of the BPVMB and BPVMB : Fe^{3+} = 1 : 3 solution at 418 nm and 460 nm. The solid lines are multiexponential fits to these kinetics.

Table 1 The values of the kinetics of transient of the BPVMB and different proportions of BPVMB : Fe^{3+} samples at 418 nm and 460 nm

Sample@418 nm	A_0 (%)	A_1 (%)	A_2 (%)	t_1 [ps]	t_2 [ps]	t_3 [ps]
BPVMB		42	58		0.36	2480
BPVMB : Fe^{3+} = 1 : 0.5	29	16	55	6.18	141.9	3062
BPVMB : Fe^{3+} = 1 : 1	27	6	67	2.46	36.8	598
BPVMB : Fe^{3+} = 1 : 2	33	9	58	0.42	10.5	840
BPVMB : Fe^{3+} = 1 : 3	30.6	10	59.4	0.68	11.4	897
BPVMB : Fe^{3+} = 1 : 5	26	25	49	1.20	22.8	801
BPVMB : Fe^{3+} = 1 : 3@460 nm		10	90		12.7	914

carrier transport channel (CT), and therefore it will have three parts of lifetimes, namely the CT (t_1), nonradiative recombination or intraband relaxation (t_2), and radiative recombination (t_3), respectively. At low concentrations of Fe^{3+} (BPVMB : Fe^{3+} < 1 : 2), the value of t_1 decreases with the content of Fe^{3+}, indicating that the process of CT though space is more faster since the Fe^{3+} gradually combines with BPVMB. Also, t_2 and t_3 are faster with an increase of Fe^{3+} because the carrier SCT transport channel gradually becomes BCT. When the ratio of BPVMB : Fe^{3+} ≥ 1 : 2, green light emission appears, indicating that the BCT channel had become the main transmission process. The kinetics of transient of BPVMB : Fe^{3+} = 1 : 3 at 418 nm, and the time of the CT process is ∼680 fs, implying that the Fe^{3+} sensing in this work is super-sensitive. While for the condition of 460 nm, there only exist two parts of lifetimes (∼12 ps from intraband relaxation and ∼900 ps from radiative recombination), which is basically consistent with the carriers' lifetime at 418 nm. This implies that an increase of the carriers of the new combining state at 460 nm is derived from the CT at 418 nm (namely the BPVMB). This result is consistent with previous results.

Detection of Fe^{3+} based on the displacement approach

The emission response of BPVMB against various metal ions showed a remarkable selectivity of Fe^{3+} binding in two stages, and the green emission starts from the molar ratio of Fe^{3+} : BPVMB that is equal to 2 : 1. However, for practical applications, a ratiometric signal is expected to be more exclusive at even lower concentrations. In addition, one of the most essential criteria for a cation probe is the ability to detect a specific cation in the presence of other competing ions. Herein, we report the detection of Fe^{3+} based on an intermolecular (through space) and intramolecular (through bond) charge transfer mechanism. In addition, we performed an experiment to detect Fe^{3+} using a displacement strategy to achieve a highly selective "off–on" type fluorescent sensor (Fig. 7d). The displacement approach was first developed to increase the emission shift of the ratiometric signal of Zn^{2+}.[27] To date, only
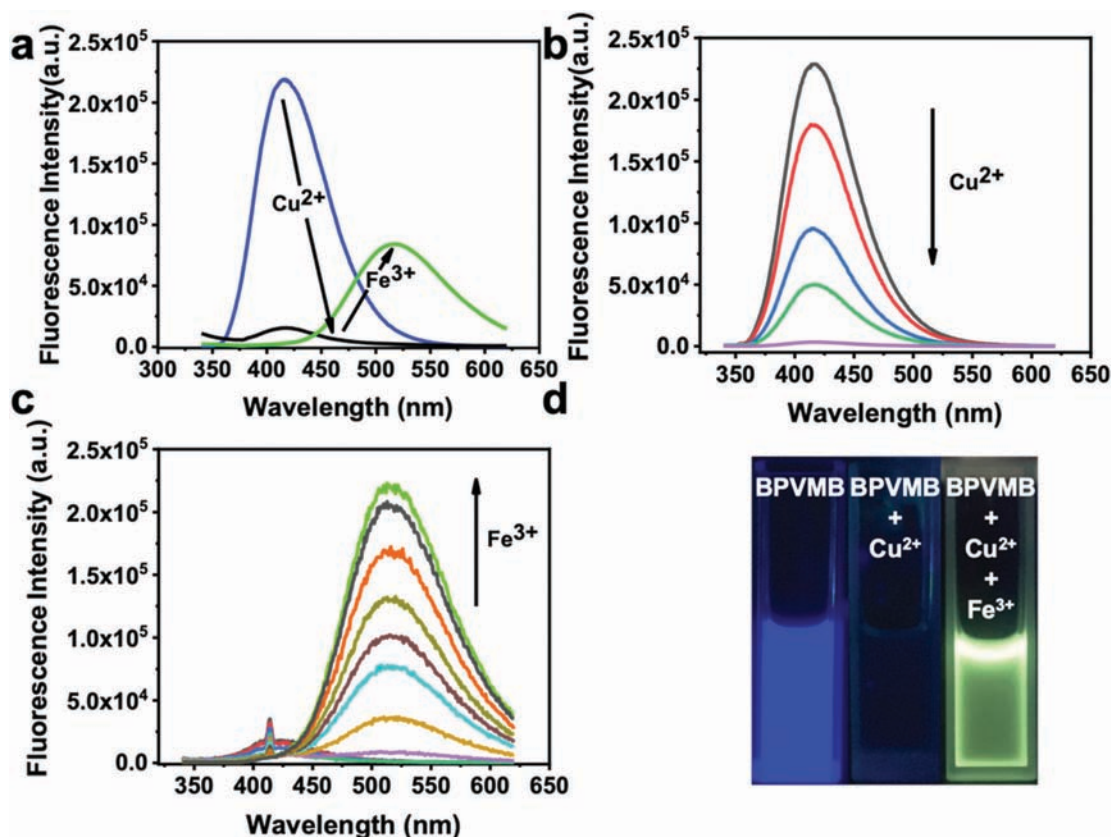

Fig. 7 (a) Emission spectra of (1) ligand BPVMB (blank), (2) BPVMB + Cu^{2+}, and (3) BPVMB + Cu^{2+} + Fe^{3+}. (b) Emission spectra of BPVMB (5 μM) in acetonitrile obtained by adding aliquots of 80 μL $CuCl_2$ (0.4 mM) solution. (c) Emission spectra of BPVMB (5 μM) in acetonitrile obtained by adding aliquots of 125 μL $FeCl_3$ (0.4 mM) solution. Excitation was at 320 nm. (d) Visible emission observed from samples of BPVMB, BPVMB/Cu^{2+}, and BPVMB/Cu^{2+}/Fe^{3+} under a UV lamp (365 nm).

14034 | J. Mater. Chem. C, 2020, **8**, 14028–14036

This journal is © The Royal Society of Chemistry 2020

a few examples of achieving such indirect cation exchange in a complex-based chemosensor is reported in the literature, especially for Fe^{3+}.[37,38] In our case, the addition of Cu^{2+} quenched the fluorescence, as shown in Fig. 7b, since the affinity of BPVMB (Fig. S7, ESI†) with Fe^{3+} ($K_d = 1.35 \times 10^{-4}$) is larger than BPVMB–$Cu^{2+}$ ($K_d = 79.9 \times 10^{-4}$) (Fig. S6, ESI†). When Fe^{3+} was added to a solution of the BPVMB–Cu^{2+} complex, Cu^{2+} was displaced by Fe^{3+} (Fig. 7c). The titration profile is based on the emission ratio at 516 and 416 nm, F_{516}/F_{416}, and the results are shown in Fig. S8 (ESI†). As can be seen, there is a linear dependence of the intensity ratios of emission at 516 nm to that at 416 nm (F_{516}/F_{416}) on the concentration of Fe^{3+}/BPVMB, which is within the range from one to three, suggesting that the addition of Fe^{3+} into the quenched BPVMB–Cu^{2+} complex leads to the emergence of green emission resulting from the formation of BPVMB–Fe^{3+}. The above results further validate that the non-fluorescent BPVMB–Cu^{2+} complex can be used as a latent off-on sensor for Fe^{3+}. In summary, the fluorescence detection limits of BPVMB for Fe^{3+} were obtained by a displacement approach. A plot of F_{516}/F_{416} *versus* [Fe^{3+}] in acetonitrile solution gave a linear relationship (Fig. S12, ESI†). The detection limit is 2.631 μM, calculated on the basis of $3\sigma/K$.[34]

Conclusions

We have synthesized a new fluorescent probe BPVMB for ratiometric and colorimetric Fe^{3+} sensing. BPVMB has the strongest affinity with Fe^{3+} among all heavy and transition metal ions and high selectivity for Fe^{3+} in two interaction modes: through space and through bond charge transfer processes. Fluorescence quenching was observed at low Fe^{3+} concentrations (below 6 μM) and then a large red-shift in emission was observed from 416 nm to 520 nm as the Fe^{3+} concentration increases from 7 μM to 20 μM, resulting from the formation of the Fe^{3+}–BPVMB complex. Also, ratiometric and colorimetric detection of Fe^{3+} with higher sensitivity can be achieved *via* a Cu^{2+} displacement approach.

Conflicts of interest

There are no conflicts to declare.

Acknowledgements

Notes and references

1 Y. Guo, L. Wang, J. Zhuo, B. Xu, X. Li, J. Zhang, Z. Zhang, H. Chi, Y. Dong and G. Lu, *Tetrahedron Lett.*, 2017, **58**, 3951–3956.

2 K. P. Carter, A. M. Young and A. E. Palmer, *Chem. Rev.*, 2014, **114**, 4564–4601.

3 Y. Jeong and J. Yoon, *Inorg. Chim. Acta*, 2012, **381**, 2–14.

4 X. Qian and Z. Xu, *Chem. Soc. Rev.*, 2015, **44**, 4487–4493.

5 T. Rasheed, M. Bilal, F. Nabeel, H. M. N. Iqbal, C. Li and Y. Zhou, *Sci. Total Environ*, 2018, **615**, 476–485.

6 D. Wu, A. C. Sedgwick, T. Gunnlaugsson, E. U. Akkaya, J. Yoon and T. D. James, *Chem. Soc. Rev.*, 2017, **46**, 7105–7123.

7 D. En, Y. Guo, B.-T. Chen, B. Dong and M.-J. Peng, *RSC Adv.*, 2014, **4**, 248–253.

8 M. W. Hentze, M. U. Muckenthaler, B. Galy and C. Camaschella, *Cell*, 2010, **142**, 24–38.

9 D. Galaris, V. Skiada and A. Barbouti, *Cancer Lett.*, 2008, **266**, 21–29.

10 L. Gambling, S. Dunford, D. I. Wallace, G. Zuur, N. Solanky, S. K. S. Srai and H. J. McArdle, *J. Physiol.*, 2003, **552**, 603–610.

11 P. Dusek, P. M. Roos, T. Litwin, S. A. Schneider, T. P. Flaten and J. Aaseth, *J. Trace Elem. Med. Biol.*, 2015, **31**, 193–203.

12 J. Cui, Y. Li, P. Yu, Q. Zhan, J. Wang, Y. Chi and P. Wang, *Int. J. Biol. Macromol.*, 2018, **108**, 412–418.

13 M. J. Wilson, J. W. T. Dekker, J. J. Harlaar, J. Jeekel, M. Schipperus and J. J. Zwaginga, *Int. J. Colorectal Dis.*, 2017, **32**, 1617–1624.

14 S. Goswami, D. Sen and N. K. Das, *Org. Lett.*, 2010, **12**, 856–859.

15 S. L. Alires, F. A. Monge, D. G. Whitten and E. Y. Chi, *Biophys. J.*, 2019, **116**, 147a.

16 J. J. Bryant, B. D. Lindner and U. H. F. Bunz, *J. Org. Chem.*, 2013, **78**, 1038–1044.

17 M. Ghaedi, K. Mortazavi, M. Montazerozohori, A. Shokrollahi and M. Soylak, *Mater. Sci. Eng., C*, 2013, **33**, 2338–2344.

18 D. Xia, S. Song, W. Gong, Y. Jiang, Z. Gao and J. Wang, *J. Food Eng.*, 2012, **113**, 11–18.

19 R. Sharma, M. Chhibber and S. K. Mittal, *RSC Adv.*, 2015, **5**, 21831–21842.

20 C. Zou, L. Gao, T. Liu, Z. Xu and J. Cui, *J. Inclusion Phenom. Macrocyclic Chem.*, 2014, **80**, 383–390.

21 P. Madhu and P. Sivakumar, *J. Photochem. Photobiol., A*, 2019, **371**, 341–348.

22 Q. Zhang, J. Wang, A. M. Kirillov, W. Dou, C. Xu, C. Xu, L. Yang, R. Fang and W. Liu, *ACS Appl. Mater. Interfaces*, 2018, **10**, 23976–23986.

23 W.-K. Dong, S. F. Akogun, Y. Zhang, Y.-X. Sun and X.-Y. Dong, *Sens. Actuators, B*, 2017, **238**, 723–734.

24 K. Ogawa, F. Guo and K. S. Schanze, *J. Photochem. Photobiol., A*, 2009, **207**, 79–85.

25 V. K. Gupta, N. Mergu and L. K. Kumawat, *Sens. Actuators, B*, 2016, **223**, 101–113.

26 Y. Zhou, F. Wang, Y. Kim, S.-J. Kim and J. Yoon, *Org. Lett.*, 2009, **11**, 4442–4445.

27 Z. Xu, K.-H. Baek, H. Na Kim, J. Cui, X. Qian, D. R. Spring, I. Shin and J. Yoon, *J. Am. Chem. Soc.*, 2009, **132**, 601–610.

28 S. K. Sahoo, D. Sharma, R. K. Bera, G. Crisponi and J. F. Callan, *Chem. Soc. Rev.*, 2012, **41**, 7195–7227.

29 X. Y. Liu, D. R. Bai and S. Wang, *Angew. Chem., Int. Ed.*, 2006, **45**, 5475–5478.

This journal is © The Royal Society of Chemistry 2020

J. Mater. Chem. C, 2020, **8**, 14028–14036 | **14035**

30 Z. M. Hudson, X.-Y. Liu and S. Wang, *Org. Lett.*, 2010, **13**, 300–303.

31 K.-L. Woon, C.-L. Yi, K.-C. Pan, M. K. Etherington, C.-C. Wu, K.-T. Wong and A. P. Monkman, *J. Phys. Chem. C*, 2019, **123**, 12400–12410.

32 P. Shen, Z. Zhuang, X.-F. Jiang, J. Li, S. Yao, Z. Zhao and B. Z. Tang, *J. Phys. Chem. Lett.*, 2019, **10**, 2648–2656.

33 G. Song, R. Sun, J. Du, M. Chen and Y. Tian, *Chem. Commun.*, 2017, **53**, 5602–5605.

34 A. Ono and H. Togashi, *Angew. Chem., Int. Ed.*, 2004, **43**, 4300–4302.

35 S. M. Saleh, R. Ali and O. S. Wolfbeis, *Chem. – Eur. J.*, 2011, **17**, 14611–14617.

36 M. Makarska-Bialokoz, *J. Fluoresc.*, 2012, **22**, 1521–1530.

37 J. Cheng, X. Zhou and H. Xiang, *Analyst*, 2015, **140**, 7082–7115.

38 Z. Li, L. Zhang, L. Wang, Y. Guo, L. Cai, M. Yu and L. Wei, *Chem. Commun.*, 2011, **47**, 5798–5800.